ACKNOWLEDGMENTS

The author would like to thank Professor T. Sakata of Science University of Tokyo for his encouragement and advice and T. Fujii for helpful discussions. He also would like to thank T. Suzuki for reading the manuscript and making suggestions.

[1]J. P. Piton and M. F. Fay, C.R. Acad. Sci. C **266**, 154 (1968).
[2]G. V. Samsonove, *Refractory Transition Metal Compound*, translated by G. E. Gurr and D. J. Parker (Academic, New York, 1955), p. 178.
[3]F. A. Sidorenko, P. V. Gel'd, and L. B. Dubrovskaya, Fiz. Met. Metalloved. **8**, 735 (1959).
[4]L. Pauling and A. M. Soldate, Acta Crystallogr. **1**, 212 (1948).
[5]R. Bucksch, Z. Naturforsch. A **22**, 2124 (1967).
[6]R. Wandji, Y. Dusausoy, J. Protas, and B. Roques, C.R. Acad. Sci. C **267**, 1587 (1968).
[7]U. Birkholz and J. Schelm, Phys. Status Solidi **34**, 177 (1969).
[8]R. M. Ware and D. J. McNeill, Proc. Inst. Electr. Eng. **111**, 178 (1964).
[9]J. Hesse, Z. Angew. Phys. **28**, 133 (1969).
[10]J. Hesse and R. Bucksch, J. Mater. Sci. **5**, 272 (1970).
[11]U. Birkholz and J. Schelm, Phys. Status Solidi **27**, 413 (1968).
[12]J. Hesse, Z. Metallkd. **60**, 652 (1969).
[13]U. Birkholz and A. Fruhauf, Phys. Status Solidi **34**, K181 (1969).
[14]T. Sakata and T. Tokushima, Trans. Nat. Res. Inst. Metals 5, 34 (1963).
[15]F. J. Morin, Phys. Rev. Lett. **3**, 34 (1959).
[16]T. Sakata, K. Sakata, and I. Nishida, Phys. Status Solidi **34**, K177 (1969).
[17]D. Adler and H. Brooks, Phys. Rev. **155**, 826 (1967).
[18]G. L. Pearson and J. Bardeen, Phys. Rev. **75**, 865 (1949).

PHYSICAL REVIEW B VOLUME 7, NUMBER 6 15 MARCH 1973

# Brillouin-Scattering Studies of Acoustoelectric Gain and Lattice Attenuation in Semiconducting CdS

U. Gelbart and A. Many
*The Racah Institute of Physics, The Hebrew University, Jerusalem, Israel*
(Received 30 June 1972)

Brillouin-scattering measurements were used to study acoustoelectric interactions in semiconducting CdS. In the GHz frequency range, a double-pulse technique described earlier was employed to suppress domain formation and thereby reduce down-conversion processes. In this manner considerable extension of the small-signal regime towards higher flux levels could be achieved. At lower frequencies, nonlinear effects were invoked to produce a propagating low-frequency domain whose attenuation and amplification were subsequently studied under small-signal conditions. Analysis of the time evolution of the spatial and frequency distribution of the amplified flux, measured under different conditions, provided accurate data on the frequency dependence of the acoustoelectric gain and the lattice attenuation over the broad range of 0.15–4 GHz. Comparison of the measured gain parameters with the small-signal theory of acoustoelectric amplification gave very good agreement throughout the frequency range studied. The lattice attenuation was found to follow the expected $f^2$ Akhiezer law at high frequencies and to vary much more slowly, if at all, in the low-frequency range (0.2–0.6 GHz). In this latter range the lattice attenuation is very low ($\sim 1$ cm$^{-1}$) and is most probably controlled by crystal imperfections. Although the studies in this paper were mostly confined to the small-signal regime, several interesting features have emerged concerning nonlinear effects. In particular, the down-converted low-frequency flux in a propagating domain was observed to lag slightly behind the high-frequency flux from which it originated. No explanation can be offered at present for this rather surprising phenomenon.

## INTRODUCTION

Acoustoelectric amplification or attenuation in piezoelectric semiconductors arises from the interaction between the rather strong ac field associated with piezoelectrically active acoustic waves and the electrons (or holes) present in the crystal.[1–4] Amplification occurs when the drift velocity imparted to the electrons by an external dc field exceeds the sound velocity. Such amplification is selective in both frequency and direction of propagation. Only phonons within a bandwidth centered around some optimal frequency and propagating in a narrow cone around the direction of electron drift are amplified. Under small-signal conditions the optimal frequency is determined by the material parameters. At larger acoustic intensities, there is usually a progressive shift in the spectrum towards lower frequencies resulting from nonlinear down-conversion pro-

cesses. The evolution of the spectrum under small- and large-signal conditions is investigated best by Brillouin-scattering measurements.[4-6] One can follow the growth and attenuation of the different frequency components of the amplified flux and thus study the various electron-phonon and phonon-phonon interactions as a function of frequency and flux intensity. Measurements of this sort have been reported for a number of semiconductors,[4,7,8] with CdS receiving particular attention.[4,9-13] So far only shear waves could be amplified acoustoelectrically and most studies were confined to this mode.

In the present work Brillouin scattering is employed to examine the validity of the small-signal theory in semiconducting CdS and to derive the frequency dependence of the lattice attenuation. At low frequencies (< 0.5 GHz) transducer measurements were successfully employed for these purposes.[4,14,15] At higher frequencies, on the other hand, although many Brillouin-scattering studies have been carried out, hardly any quantitative data are available on the small-signal regime to permit a systematic comparison with theory. This is largely due to the strong tendency of the amplified flux in CdS to be highly concentrated in narrow domains.[3,4] Nonlinear processes are very pronounced in such domains,[4,13] so that by the time the acoustic flux has been amplified to a detectable level it is at best near the limit of the small-signal region or, as happens more often, well into the large-signal regime. This feature is probably responsible, at least in part, for the accent being placed on nonlinear effects, and by now considerable information has become available on such processes.[4,7-10,13] Another difficulty in deriving the gain parameters is the predominant effect of nonhomogeneity on the amplification process. Because of the particularly strong electron-phonon coupling in CdS, a few-percent variation in the electron drift velocity along the sample introduced by inhomogeneities is usually sufficient to make a quantitative analysis of the data unfeasible. In both respects, the situation is far better in most of the other materials studied. This contributed in no small measure to the success of Palik and Bray[8] in obtaining a fairly detailed characterization of the small-signal regime in $n$-GaAs, even though domains were present and the samples were not too homogeneous.

The main factor that made the present measurements feasible was the use of the double-pulse scheme described earlier.[13] In this scheme, domain formation is almost entirely suppressed and with it the excessive parametric down-conversion. Small-signal conditions can then be maintained up to at least three orders of magnitude above the detectable level. Using, furthermore, highly uniform samples, we were able to determine the gain parameters rather accurately over the frequency range 0.2–4 GHz. The results obtained are in very good agreement with the small-signal theory.[1] The measurements also yielded important information on the frequency dependence of the lattice attenuation. Such attenuation results from nonelectronic interaction of the amplified flux with thermal phonons[16,17] and, in CdS, should be expected to increase quadratically with frequency in the range studied (Akhiezer loss[18,19]). At high frequencies, this quadratic dependence is indeed observed, at variance with findings of other workers.[11,20] At low frequencies (0.2–0.6 GHz) the lattice attenuation is found to vary more slowly with frequency and is compatible—within the margin of error—with transducer measurements.[15] In this range the attenuation is very low (around 1 $cm^{-1}$) and as a result is more sensitive to crystal imperfections.

We review briefly the small-signal theory of acoustoelectric amplification. For sufficiently conducting material, the energy gain in the direction of electron drift can be expressed as[1,21,22]

$$\alpha(f) = \alpha_0(f)\gamma , \tag{1}$$

where

$$\gamma = v_d/v_s - 1 , \tag{2}$$

$v_d$ being the electron drift velocity and $v_s$ the shear-wave sound velocity. For CdS in the frequency range of interest, the product $ql$ of phonon wave vector and electron mean free path is small compared to unity. Under these conditions the frequency dependence of the field-free amplification factor $\alpha_0(f)$ is given (in units of reciprocal length) by[1]

$$\alpha_0(f) = 2\pi K^2 v_s^{-1} f_D (f/f_m + f_m/f)^{-2} , \tag{3}$$

where $K^2$ is the electromechanical coupling constant (= 0.036 in CdS), $f_D = v_s^2/2\pi D$ is the diffusion frequency and $f_m = (f_c f_D)^{1/2}$ is the frequency of maximum gain. Here $D = \mu kT/e$ is the diffusion constant, $f_c = \sigma/2\pi\epsilon$ is the dielectric relaxation frequency, $\sigma$ is the material conductivity, $\mu$ the electron mobility, and $\epsilon$ the dielectric constant. In CdS at room temperature $\alpha_0(f_m)$ is about 200 $cm^{-1}$ and is much larger than the corresponding values for GaAs (typically 2–20 $cm^{-1}$) and InSb (0.2–0.4 $cm^{-1}$ at 77 K). The *net* gain is given by

$$\alpha_n(f) = \alpha_0(f)\gamma - \alpha_l(f) ,$$

where $\alpha_l$ is the nonelectronic lattice attenuation. Since $\alpha_l$ is a monotonically increasing function of $f$, the frequency of maximum *net* gain $f_N$ is shifted somewhat below $f_m$.

Operationally, the small-signal or weak-flux regime covers the range of flux densities for which $\alpha_0$ and $\alpha_l$ are to a good approximation flux independent. In the present studies we shall be con-

cerned throughout with small-signal conditions. At low frequencies, however, $\alpha_0$ is too small to permit linear amplification of thermal noise to a sufficient level. Similarly to other workers[8,9,20,23,24] we therefore invoke nonlinear effects to generate parametrically a propagating low-frequency domain. The amplification and/or attenuation of this domain is subsequently studied *under small-signal conditions* as a function of frequency.

## EXPERIMENTAL PROCEDURE

The time, spatial, and frequency distribution of the amplified shear-wave flux has been studied by Brillouin scattering. A parallel monochromatic light beam (for which the crystal under study is transparent) is focused on the sample. Most of the light is transmitted through but a small fraction is scattered out of the incident direction by phonon emission (Stokes scattering) or absorption (anti-Stokes). The scattering process is governed by momentum and energy selection rules relating the frequencies, wave vectors, and polarization of the incident and scattered light with those of the phonons involved in the scattering. In particular, each pair of incident and scattering angles corresponds to phonons of a single frequency. The frequency shifts of the scattered light are very small. Moreover, for the long-wavelength phonons amplified acoustoelectrically there is negligible dispersion, so that with the sound velocity known only scattering angles (and not frequency shifts) need be measured. Thus, since the scattered-light intensity is directly proportional to the acoustic flux density, the phonon frequency spectrum can be obtained by measurements at different pairs of incident and scattering angles.

In optically isotropic crystals the selection rules are quite simple.[25] In birefringent crystals such as CdS, on the other hand, the relationship between the incident and scattered angles and the phonon frequency is more involved.[26,27] This is because the refractive index, which determines the magnitude of the wave vector within the crystal, depends on the polarization and direction of propagation of the light, both of which are usually different for the incident and scattered light. In CdS one is interested in piezoelectrically active shear waves, i.e., polarized along the $c$ axis. It is customary to chose the simplest scattering geometry, namely, the incident light beam perpendicular to the $c$ axis with its polarization either normal (ordinary configuration) or parallel (extraordinary) to the $c$ axis. In either case the polarization of the scattered beam is rotated by 90° with respect to that of the incident beam.[25-27]

Almost all workers[4] used the ordinary configuration but we preferred the extraordinary configuration because of an important advantage to be discussed below. Figure 1 illustrates the momentum selection rule in the extraordinary configuration for absorption of phonons propagating along the length of the sample ("on-axis" flux). The radii of the two arcs shown represent the magnitudes $k_0 n_{ex}$ and $k_0 n_{or}$ of the wave vector within the crystal for light of a given frequency (wave vector $k_0$ in vacuum) when polarized parallel (refractive index $n_{ex}$) and perpendicular ($n_{or}$) to the $c$ axis. Thus, in the extraordinary configuration, the incident-light wave vector $\vec{k}_i$ (incident angle $\theta_i$) terminates on the outer circle ($n_{ex} > n_{or}$). Upon scattering by a shear-wave phonon, the plane of polarization is rotated by 90° and (neglecting the small frequency shift) the scattered-light wave vector $\vec{k}_s$ must terminate on the inner circle. It is seen that for each wave vector $\vec{k}_i$, two on-axis phonon wave vectors $\vec{K}^-$ and $\vec{K}^+$ can satisfy the momentum selection rule, giving rise to two scattered-light wave vectors $\vec{k}_s^-$ and $\vec{k}_s^+$ (scattering angles $\theta_s^+$ and $\theta_s^-$). In CdS, as in most crystals, $\Delta k/k = \Delta n/n \ll 1$ (where $\Delta k = k_i - k_s$, $\Delta n = n_{ex} - n_{or}$), so that to a good approximation the momentum selection rule can be written as

$$\sin\theta_i = K/2k_i + \Delta k/K\,,$$

$$\sin\theta_s = K/2k_s - \Delta k/K\,.$$

The incident and scattering angles *outside* the sample $\theta_{i0}$ and $\theta_{s0}$ are readily obtained from the inner angles $\theta_i$ and $\theta_s$ by Snell's law.

In practice the situation is somewhat more involved. The amplified acoustic flux is not confined to the on-axis direction but is contained in a cone around this direction. Also the incident light beam is not strictly monochromatic and has

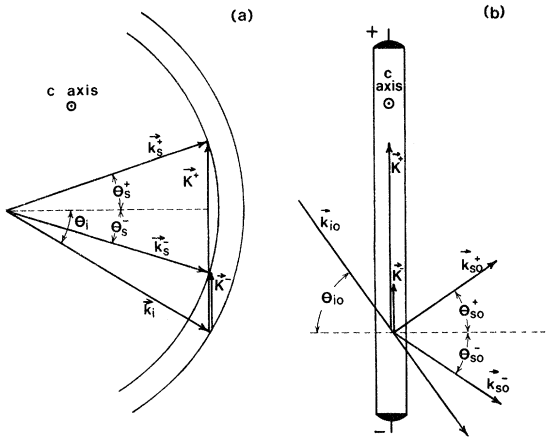


FIG. 1. Brillouin scattering in extraordinary configuration. Momentum selection rule for phonon absorption illustrated at left, while sample geometry shown at right. At left: incident and scattering angles are internal; at right: external.

a finite divergence ($\Delta\theta_{i0}$), while the scattered-light detecting system has a nonvanishing aperture ($\Delta\theta_{s0}$). For a given set of experimental conditions, however, one can readily evaluate the off-axis cone ($\Delta\Omega$) and hence the frequency bandwidth of the phonons involved in the measured scattered-light intensity (see below).

Figure 2 is a schematic diagram of the optical system used. A He-Ne laser beam is focused on the CdS sample. The width of the light spot on the sample surface is 0.15 mm. The incident-light polarization and the $c$ axis are both normal to the plane of the diagram (extraordinary configuration). The scattered light is passed through an analyzer to select light with polarization rotated by 90° in the scattering process. (The analyzer rejects more than 99% of the undesired light scattered by surface roughness.) The sample is on a rotating table which serves to determine the incident angle ($\theta_{i0}$) while the photomultiplier is mounted on a concentrically rotating arm used to select the desired scattering angle ($\theta_{s0}$).

For each pair of angles $\theta_{i0}$, $\theta_{s0}$ corresponding to a certain phonon frequency, the ratio $I/I_0$ of scattered to incident light intensity is proportional to the acoustic flux density at that frequency.[25,27] The factor of proportionality is expected to vary with the angle of incidence because of differences in surface reflectivity, in the optical path of the light within the sample, and in the frequency bandwidth of the phonons scattering into the photomultiplier aperture. It can be shown,[27] however, that for sufficiently small values of $\Delta\theta_{i0}$, $\Delta\theta_{s0}$, this factor is essentially independent of incidence angle over the entire phonon frequency range that can be studied. For He-Ne laser light ($\lambda = 6328$ Å) in CdS, this range extends from 0.15 to about 5 GHz.

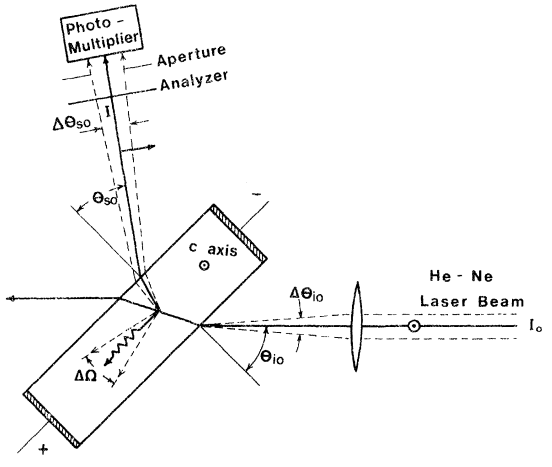


FIG. 2. Schematic diagram of optical system used in Brillouin-scattering measurements. $\Delta\theta_{i0}$ is divergence of incident light beam and $\Delta\Omega$ is cone angle of phonon beam scattering into aperture $\Delta\theta_{s0}$ of photomultiplier.

In order to obtain the phonon spectrum at a given point of the sample it is necessary that the incident light transverse, as much as possible, the same region of the sample at all the frequencies monitored. Obviously this requirement cannot be fully realized because different frequencies require different incidence angles. In the ordinary configuration a variation of about 20° in the *internal* incidence angle ($\theta_i$) is necessary to cover the spectrum, whereas in the extraordinary configuration used in the present measurements only a 10° variation suffices. This advantage of the extraordinary configuration is particularly important when narrow flux domains are studied. In CdS, the flux in the domain grows very rapidly with distance,[4] so that changes in the optical path of the incident beam can introduce large errors in the measurement.

An important feature of birefringent materials is that they permit measurements of the flux density at two different phonon frequencies for the *same* angle of incidence (see Fig. 1). For both frequencies an identical region of the sample is involved, the only difference being in the position of the photomultiplier. This is particularly useful in studies of nonlinear processes in very narrow flux domains, when one wishes to compare the time and spatial profile of the domain at the pump frequency and at some lower frequency of the down-converted flux (see Fig. 10 below).

Phonon amplification is produced by short repetitive current pulses so that Brillouin-scattered light reaches the photomultiplier in brief flashes. The photomultiplier output is connected to an electrometer which averages these flashes and produces a dc signal. In order to eliminate the continuous light scattered from surface roughness, the photomultiplier was gated so as to respond only at controlled time intervals (usually of 50-nsec duration) synchronized with the amplifying current pulses. In this manner considerable enhancement in signal-to-noise ratio has been obtained, permitting the measurement of Brillouin-scattered-light intensities as low as eight orders of magnitude below the incident-light intensity. (For such low flux densities, the pulse-on signal becomes comparable to the fluctuations in the pulse-off signal associated with the light scattered by surface roughness.)

The spatial resolution of the flux distribution is determined by the width of the incident beam and its path within the sample. In our system it varies between 0.15 and 0.25 mm over the phonon-frequency range studied (0.2–4 GHz). The spectral resolution for the 1° photomultiplier aperture used is less than 40 MHz. The cone angle of the off-axis phonon beam scattering into the photomultiplier is less than 0.2° in the range 4–0.5

GHz, and increases from 0.2° to 3° in the range 0.5–0.2 GHz.

Acoustoelectrically amplified flux in semiconducting CdS is usually found to be concentrated in narrow domains ($\lesssim 0.2$ mm) propagating with sonic speed from the cathode to the anode.[3,4] As has been shown in a previous publication,[13] the flux domains can be eliminated by the use of a double-pulse scheme, probably through the suppression of the piezoelectric shock[28,29] attending the onset of the current pulse. In this scheme the amplitude of the first pulse is set below the threshold for net acoustoelectric gain. After a sonic transit time or so, when any flux produced by the onset of the first pulse has left the sample, a second pulse of much lower amplitude is superimposed on the first. Conditions of net acoustic gain are established at the onset of the second pulse, $\gamma$ then corresponding to the combined amplitude of the two pulses. In this manner the effect of the shock is largely suppressed and the amplified flux originates almost entirely from the thermal-equilibrium phonon distribution within the crystal.

The double pulse has been obtained from two pulse generators by the use of a simple addition network. A Velonex pulse generator supplied the second pulse. Its fast rise time (~35 nsec) is an essential feature in determining the time and spatial distribution of the amplified flux. The acoustic gain in CdS is very sensitive to variations in the current amplitude. Accordingly, in some cases an electronic stabilizer has been employed to stabilize the pulse amplitude to better than 0.1%. Such stabilization served also to better approximate constant-current conditions and in this manner minimize current feedback effects.

The measurements were carried out on semiconducting CdS samples (5–10 Ω cm) of rectangular shape, having typical dimensions of $0.5\times2\times10$ mm. The $c$ axis was perpendicular to the long dimension and parallel to the two larger faces, which were optically polished. Ohmic end contacts were applied by indium solder. The samples were carefully checked for resistivity homogeneity and in most measurements only those uniform to better than 1–2% were chosen.

## RESULTS AND DISCUSSION

Brillouin-scattering data obtained by the double-pulse technique on a highly uniform CdS sample are shown in Fig. 3. Here the spatial distribution of the amplified on-axis flux at several instants following the onset of the second pulse ($t=0$) are plotted (on a semilog scale) for two values of the combined current amplitude (two values of $\gamma$). The incident and scattering angles in this measurement correspond to the frequency of maximum net gain $f_N$, which for this particular sample is 2.5 GHz. The ordinate in this figure represents the ratio $I/I_0$ of the scattered to incident light intensities, while the abscissa delineates the distance of the light spot from the cathode. It is seen that at each instant $t$ shorter than the sonic transit time $L/v_s$, the flux density increases exponentially with distance $x$ from the cathode up to the point $x=v_st$. From thereon the flux remains nearly constant all the way to the anode ($x=L$). (The small undulations around the constant level are mainly due to slight resistivity nonuniformities, as will be discussed below.) For $t\geq L/v_s$ (=4.45 μsec) the flux distribution is exponential throughout the length of the sample and remains fixed with time (steady-state conditions).

This behavior provides conclusive evidence that under the conditions of the measurement (double pulse) the amplified flux originates entirely from the bulk thermal-equilibrium phonon distribution. From the absence of a peak in the spatial distribution at the points $x=v_st$, one immediately concludes that the cathode does not act as a source of acoustic flux (produced by shock excitation at the onset of the second pulse or otherwise). At any instant $t$, the flux plateau ($x\geq v_st$) must have originated from points *within* the sample, where the only source of flux can be the uniform thermal background.

The integrated flux density in the measurements of Fig. 3 has been kept sufficiently low so that departures from constant-current (constant-gain) conditions are negligible. Under these conditions and in the absence of shock excited flux, the small-signal amplification of the uniform thermal background should give rise in a homogeneous sample to the following time and spatial flux distribution[30,31]:

$$\phi(x,\ t)=\phi_0[1+(\alpha_0+\alpha_l)/\alpha_n]\,e^{\alpha_n x}, \qquad x\leq v_st \tag{4a}$$

$$\phi(x,\ t)=\phi_0[1+(\alpha_0+\alpha_l)/\alpha_n]\,e^{\alpha_n v_s t}, \qquad x\geq v_st. \tag{4b}$$

Here $\phi_0$ and $\phi(x,\ t)$ represent, respectively, the thermal-equilibrium and amplified flux densities enclosed within a narrow cone in the direction of electron drift and in a narrow frequency bandwidth around the frequency under study; $\alpha_0$, $\alpha_l$, and $\alpha_n$ are as defined above [see Eqs. (1) and (3)]. [In Eqs. (4) a term $(\alpha_0+\alpha_l)\phi_0/\alpha_n$ has been omitted since in practice it is at least several orders of magnitude smaller than the other terms.] The form of the flux distribution represented by Eqs. (4) can be understood by simple physical arguments. At a given instant $t$ ($<L/v_s$), the flux at any point $x\geq v_st$ originates from thermal flux ($\phi_0$) *within* the sample and is amplified along the *same* distance $v_st$. Since both $\phi_0$ and $\alpha_n$ are uniform, $\phi(x,\ t)$ in this region should be independent of position (the plateau region). For $x<v_st$, on the

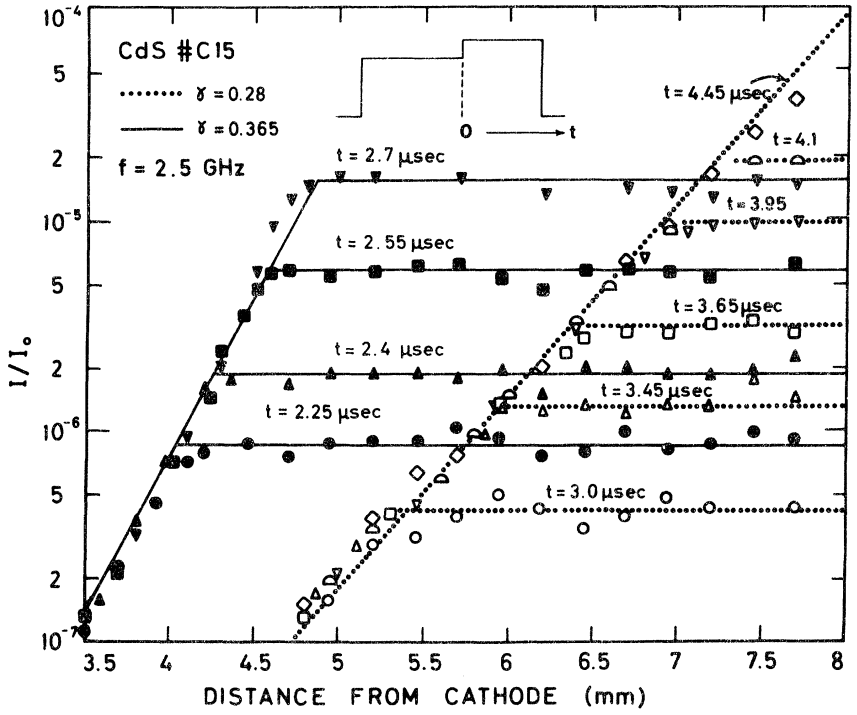


FIG. 3. Spatial distribution of amplified flux at frequency of maximum net gain $f_N$ for two values of $\gamma = v_d/v_s - 1$, as obtained by double-pulse measurements. Drift velocity $v_d$ derived from amplitude of second pulse while $v_s = 1.77 \times 10^5$ cm/sec for piezoelectrically active shear waves in CdS (Ref. 4). Different curves correspond to different instants following onset of second pulse ($t = 0$). Ordinate represents ratio $I/I_0$ of scattered to incident-light intensity; abscissa delineates distances $x$ of light spot from cathode. Double-pulse configuration used is shown by diagram. (Electron concentration and mobility in CdS sample $3.3 \times 10^{15}$ cm$^{-3}$ and 280 cm$^2$/V sec.)

other hand, amplification takes place over a distance less than $v_s t$, and $\phi(x, t)$ is expected to increase exponentially with $x$. The first term in the preexponential brackets in Eqs. (4) represents the amplified flux in the wave front starting at $t = 0$ from the point $x - v_s t$ (or the cathode if $x < v_s t$) with initial level $\phi_0$, while the second term represents amplified flux added to this front as it propagates down the sample by thermal generation.

Actually, Eqs. (4) should be modified to take into account possible flux reflection at the contact boundaries.[31] In CdS, however, $(\alpha_0 + \alpha_l)/\alpha_n \gg 1$, and the effect of such reflections may be neglected.

The observed time evolution of the flux distribution shown in Fig. 3 is in complete agreement with Eqs. (4). Thus, an analysis based on Eqs. (4) of such flux distribution curves, measured under different drift currents and at different acoustic frequencies, can yield the frequency dependence of $\alpha_0$ and $\alpha_l$. For example, the slopes of the expotential lines, corresponding to the two values of $\gamma$ shown, lead to $\alpha_0 = 160$ cm$^{-1}$ and $\alpha_l = 23$ cm$^{-1}$ at the frequency monitored (2.5 GHz).

It should be noted in Fig. 3 that small-signal conditions (for which $\alpha_0$ and $\alpha_l$ are independent of flux level) prevail over nearly three orders of magnitude of detectable flux densities. As a result $\alpha_0$ and $\alpha_l$ can be determined rather accurately. With a conventional single-pulse operation, regenerative processes and parametric down conversion, occurring within the domains, curtail drastically the small-signal range.[13]

Similar results of the flux distribution at the frequency $f_N$ of maximum net gain taken on another highly uniform sample are shown in Fig. 4, this time for the two polarities of the applied double pulse. In both cases the current amplitudes (and hence $\gamma$) are identical. Here again the distribution is in accord with Eqs. (4). The complete symmetry for the two polarities is further indication for the uniformity of the sample.

The effect of nonuniformity on the flux distribution is illustrated in Fig. 5. The results here were obtained on the sample of Fig. 4 after slightly polishing it into a wedge shape. The over-all variation in cross section from one end of the sample to the other amounted to only 4%, yet the departures of the distribution curves from Eqs. (4) are quite substantial. This is a result of the great sensitivity of the gain $\alpha$ in CdS to nonuniformities, owing to the large value of the field-free amplification factor $\alpha_0$. It can readily be shown that the relative change in the local value of $\alpha$ resulting from changes along the sample in the mobility $\mu$, in the electron concentration $n$, and in the cross section $A$, is given by [see Eqs. (1)–(3)]

$$\frac{\Delta\alpha}{\alpha} = -\left(\frac{\Delta\mu}{\mu} + \frac{1 - f/f_m}{f/f_m + f_m/f}\,\frac{\Delta n}{n} + \frac{1+\gamma}{\gamma}\,\frac{\Delta(nA)}{nA}\right), \tag{5}$$

where $f_m$ is the frequency of maximum gain. The first term, which reflects the effect of a mobility variation on $\alpha_0$ [see Eq. (3)] can be neglected in our samples. The second term represents the

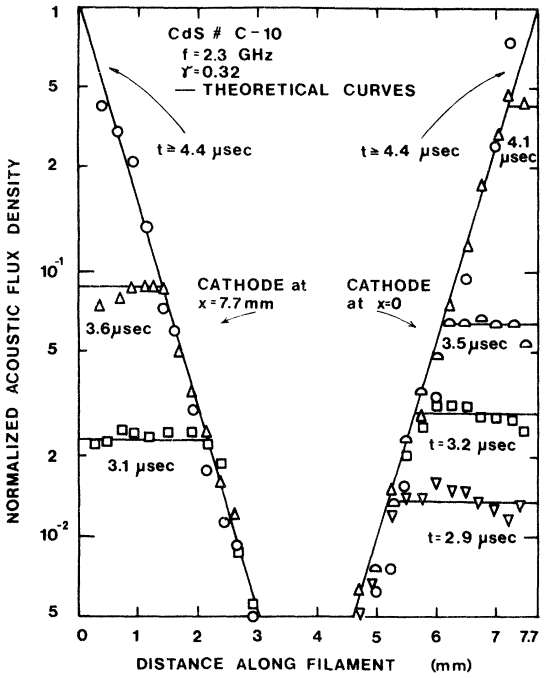


FIG. 4. Spatial distributions of amplified flux at $f=2.3$ GHz for two polarities (but same amplitude) of applied double pulse. Different curves correspond to different instants following onset of second pulse ($t=0$). (Electron concentration and mobility in CdS sample $3.6\times10^{15}$ cm$^{-3}$ and 290 cm$^2$/V sec.)

change in $\alpha$ due to the change in $f_m$: With increasing $n$, $f_m$ shifts to higher frequencies so that the gain at the frequency studied ($f$) decreases. The third term represents the effect of the change in drift velocity arising from variation in either $n$ or $A$: Increasing $nA$ at any point reduces $\gamma$ and hence $\alpha$ at that point. Obviously the relative change in the *net* gain $\alpha_n=\alpha-\alpha_l$ is larger than $\Delta\alpha/\alpha$ (by the factor $\alpha/\alpha_n$).

In semiconducting CdS the last term in Eq. (5) constitutes the major contribution to $\Delta\alpha/\alpha$. This is because $(1+\gamma)/\gamma$ is usually larger than 3-4 while in the frequency range studied ($f<f_m$) the coefficient of $\Delta n/n$ is less than 0.2. Thus, any resistivity nonhomogeneity along the sample can be legitimately compensated for by suitable "tailoring" of the cross section along the sample. The converse procedure has been employed in Fig. 5, where a uniform sample has been altered into a nonuniform one by introducing a 4% over-all variation in cross section. This corresponds to a change of about 40% in the net gain![32] The cross section decreases continuously and hence the net gain $\alpha_n$ increases from the left end of the sample ($x=0$) to the right end. As a result, when the contact $x=0$ is made the cathode, the distribution curves for $x\leq v_st$ are superexponential, while those for $x\geq v_st$ are no longer level but slope upwards. For the opposite polarity, the curves are subexponential for $L-x\leq v_st$ and sloping downwards for $L-x\geq v_st$ ($L$ being the length of the sample). The solid curves in Fig. 5 were calculated from Eqs. (4), suitably modified to include the 4% nonuniformity. Use was made of the independently measured values of $\mu$ and $n$, and of the parameters $\alpha_0$, $\alpha_l$ as derived from the data of Fig. 4. The fit between experiment and theory is seen to be quite good. Measurements of flux distributions for the two polarities, especially at $x\geq v_st$ (and $L-x\geq v_st$), obviously provide a very sensitive tool for detecting resistivity nonhomogeneities.

The flux distributions on the left-hand side of Fig. 5 do not represent a propagating domain. However, such distributions can result in a domain at higher flux densities. Two mechanisms then become operative. One is a feedback effect. At sufficiently high flux levels, constant-current conditions can no longer be maintained: The increasing resistance of the sample associated with the growing flux continuously reduces the current and hence the acoustic gain. Thus, flux arriving at the point $x$ in the sample at the sonic time $x/v_s$ would have been amplified under higher gain than flux arriving at that point at a later time. This would give rise to a propagating domain, whose extrapolated point of origin is the cathode boundary, and hence to current oscillations Another mech-

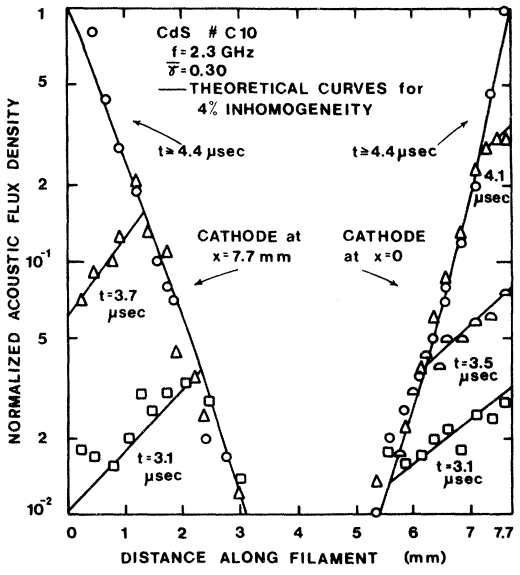


FIG. 5. Time and spatial distributions in sample of Fig. 4 after introducing 4% over-all variation in cross section from one end of sample to the other. Average $\gamma$ value ($\bar{\gamma}=0.30$) is same for two polarities. Lines represent calculated distributions taking into account cross-section variation.

anism is a regenerative process[33] known to occur in CdS under large-signal conditions. At high flux densities the gain becomes an increasing function of flux density, a process that sharpens any peak present in the flux distribution.

The measurements described above were interpreted on the tacit assumption that as far as the flux growth process is concerned, the double-pulse scheme is completely equivalent to the conventional single-pulse procedure in the absence of shock excitation. Hence the use of Eqs. (4) which, strictly speaking, are valid only for amplification from thermal background noise under single-pulse operation. The conditions under which our assumption is valid will now be examined. In the absence of a drift current (thermal equilibrium) the flux attenuation rate $(\alpha_0+\alpha_l)\phi_0$ is balanced by the generation rate. Upon the application of the first pulse, the generation rate remains unaltered but the attenuation rate *decreases* even though the pulse amplitude is below threshold for net gain.[34] As a result, the flux density during the first pulse is higher than the thermal-equilibrium level. A calculation similar to that used in deriving Eqs. (4) leads to the following expressions for the flux distribution at time $t$ following the onset of the *second* pulse:

$$\phi(x,\ t)=[1+(\alpha_0+\alpha_l)/\alpha_n]\,\phi_0 e^{\alpha_n x},\qquad x\leq v_s t$$

$$\phi(x,\ t)=\{[1+(\alpha_0+\alpha_l)/\alpha_{n1}]\,(e^{\alpha_{n1}(x-v_s t)}-1)+1+(\alpha_0+\alpha_l)/\alpha_n\}\,\phi_0 e^{\alpha_n v_s t},\quad x\geq v_s t \tag{6}$$

where $\alpha_{n1}$ is the net gain during the first pulse ($\alpha_{n1}\equiv\alpha_1-\alpha_l$) and $\alpha_n$ is, as before, the net gain during the second pulse. In the derivation of Eqs. (6) it has been assumed that the duration of the first pulse exceeds the sonic time through the sample, as was the case in practice. Here again flux reflection at the contact boundaries[31] can and has been neglected.

From Eqs. (6) one expects the flux distribution for $x\leq v_s t$ to be independent of $\alpha_{n1}$. In particular, it should coincide with the distribution when the amplitude of the first pulse is zero (single-pulse operation). For $x>v_s t$, on the other hand, the plateau of Eq. (4b) is replaced (for $\alpha_{n1}\lesssim 0$) by a moderate rise as the anode is approached. This behavior is well illustrated by the distribution curves of Fig. 6 measured (at $f=2.5$ GHz) with the double-pulse technique. Each set of points has been obtained for a different value of $\gamma_1(\equiv\alpha_1/\alpha_0)$, with $\gamma$ of the second pulse held at the constant value of 0.245. The solid lines have been calculated from Eqs. (6) on the basis of the sample's parameters and the values of $\alpha_0$ and $\alpha_l(\equiv\alpha_0\gamma_l)$ derived from measurements on a neighboring sample cut from the same ingot. A small correction has been applied in the calculation to take into account the slight nonuniformity in the sample as exhibited, for example, at $x>v_s t$ by the sloping line for $\gamma_1=-0.085$. The fit of the experimental points is reasonably good in view of the uncertainty in the value of $\alpha_l$ (derived from another sample) which can introduce a large error into the calculated curves.

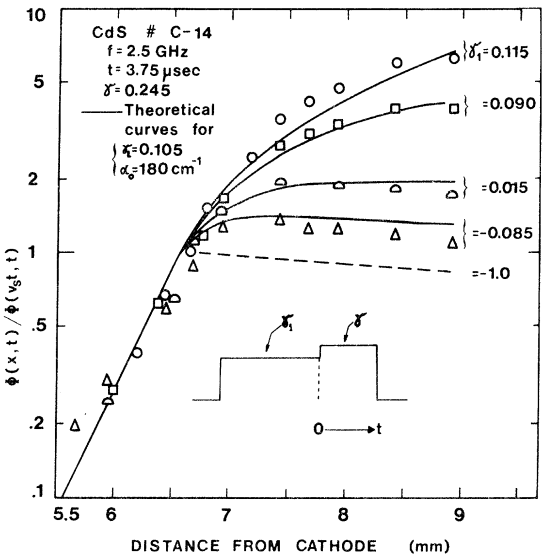


FIG. 6. Spatial distributions of amplified flux at fixed time following onset of second pulse for different amplitudes of first pulse (different $\gamma_1$ values). Amplitude of second pulse (and hence $\gamma$) held fixed. Solid curves calculated from Eqs. (6) for the different $\gamma_1$ values. Dashed curve ($\gamma_1=-1$) corresponds to zero amplitude of first pulse. Experimental values and theoretical curves normalized to unity at $x=v_s t$. (Electron concentration and mobility in CdS sample $3\times10^{15}$ cm$^{-3}$ and 280 cm$^2$/V sec.)

The distribution for $\gamma_1=-0.085$ is very close to that given by Eqs. (4) (single-pulse operation) and in all measurements of the gain parameters $\gamma_1$ has been kept below this value.

The data used in determining the frequency dependence of $\alpha_0$ and $\alpha_l$ in the spectral range around the frequency of maximum *net* gain $f_N$ are shown in Figs. 7 and 8. In all cases the measurements were restricted, as above, to small-signal conditions. In Fig. 7 the spatial distributions of the amplified flux at different frequencies are plotted for fixed values of $\gamma$ and $t$. The results are similar to those of Fig. 3 (which correspond to a single frequency) but only the range $x<v_s t$ is shown here. Some of the curves have been displaced vertically to facilitate the presentation. It is seen that at all frequencies studied the curves are exponential, the slopes of which yield the net gain $\alpha_n(f)$ through the use of Eq. (4a). The frequency and the derived value of $\alpha_n$ are marked near each curve. The net gain is maximal for $f=2.5$ GHz which, as expected,

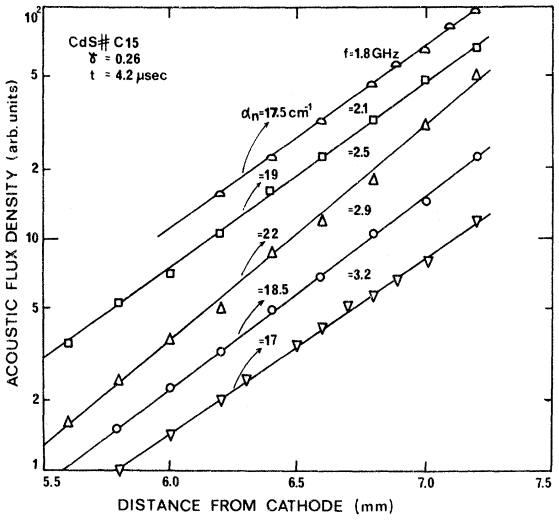


FIG. 7. Exponential rise with distance $x$ of amplified flux at different frequencies for fixed $\gamma$ and fixed time following onset of second pulse ($x < v_s t$).

is also the frequency where maximum flux intensity is observed (see Fig. 15 below).

In order to determine $\alpha_0(f)$ and $\alpha_l(f)$, additional data are required. These were obtained by measurements of the flux density $\phi$ at a fixed time $t$, anywhere in the plateau of Fig. 3 ($x > v_s t$), as a function of $\gamma$. Rewriting Eq. (4b) in the form

$$\phi(x,\ t) = [(\gamma+1)/(\gamma-\gamma_l)]\phi_0 e^{-\alpha_l v_s t}\, e^{\alpha_0 v_s t \gamma},$$

$$x \geq v_s t \qquad (4b')$$

one notes that the $\phi$-vs-$\gamma$ curve should not be strictly exponential because the preexponential term is also a function of $\gamma$. A simple procedure for deriving $\alpha_0$ and $\gamma_l (\equiv \alpha_l/\alpha_0)$ from the experimental curves is by successive approximations. An approximate value is first obtained for $\alpha_0$ from the $\phi$-vs-$\gamma$ curve. Next, an approximate value of $\gamma_l$ is calculated by combining this result with the value of $\alpha_n$ derived (at the same frequency) from the data of Fig. 7. The experimental results are then replotted in the form $[(\gamma-\gamma_l)/(\gamma+1)]\phi$ vs $\gamma$ and a new value for $\alpha_0$ is obtained from the slope. The process is repeated until convergence is attained. Usually only a few cycles of successive approximations are required. The curves obtained in this manner are shown in Fig. 8 for several frequencies. For convenience in presentation, some of the curves have been displaced vertically. The values derived for $\alpha_0(f)$ are indicated near the curves while those of $\alpha_l$ are included in Fig. 14 below.

The frequencies studied above are within the bandwidth amplified under small-signal conditions. At lower frequencies, $\alpha_0(f)$ is too low to permit small-signal amplification of thermal background to a sufficient level. Hence such flux must be introduced into the sample by other means before its amplification and attenuation can be measured. A convenient way of achieving this aim is to make use of nonlinear processes taking place under large-signal conditions.[8,9,20,23,24] A short, large-amplitude pulse is applied in order to produce a high-intensity propagating domain near the cathode. The low-frequency flux domain generated by parametric down conversion is then either allowed to decay under zero-field conditions or else is amplified by a second pulse as it propagates towards the anode. Results obtained by the former procedure are shown in Fig. 9. Here the spatial distributions at 2.5 GHz (solid curves) and at 0.28 GHz (dashed curves) are plotted for different instants following the termination of the pulse. At the higher frequency, the flux consists of a propagating domain (represented by the peaks at $x = v_s t$) superimposed on a broad, noise-originating distribution. The flux in both distributions is very strongly attenuated. At the lower frequency, on the other hand, practically all the down-converted flux is concentrated in a domain, slightly displaced spatially from the high-frequency domain and much more weakly attenuated. The peak-intensity decay is seen to be exponential over most of the sample's length. Small-signal conditions are expected to prevail over this range since most of the high-frequency flux has disappeared by then

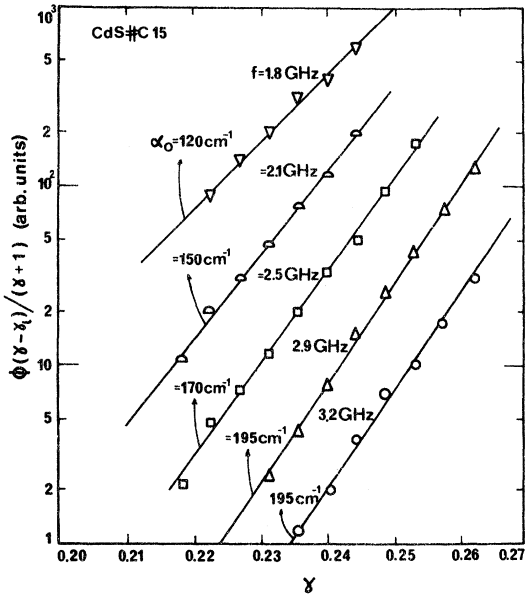


FIG. 8. Semilog plots of $\phi(\gamma-\gamma_l)/(\gamma+1)$ vs $\gamma$ for different frequencies. Flux density $\phi$ refers to amplified flux at fixed time $t$ following onset of second pulse and is measured at plateau region ($x > v_s t$).

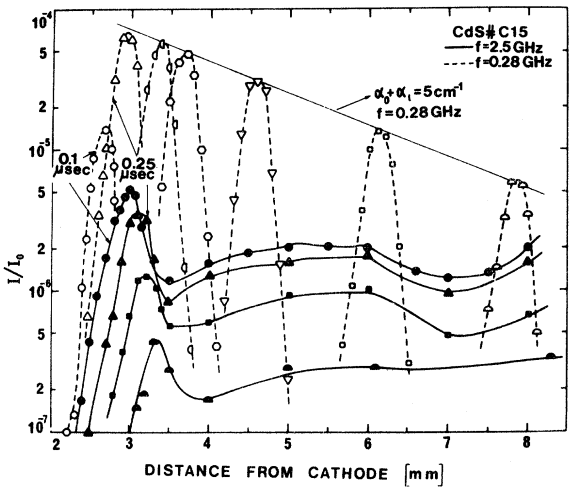


FIG. 9. Spatial flux distribution at 2.5 GHz (solid curves) and at 0.28 GHz (dashed curves) for different instants following termination of short large-amplitude pulse.

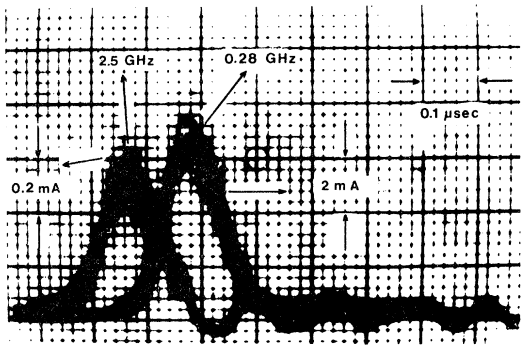


FIG. 10. Oscillogram display of the flux domains of Fig. 9. Two traces represent photomultiplier output for two scattering angles corresponding to 2.5 and 0.28 GHz. Incident angle and position of light spot are same for two frequencies. (Current scales are different for two traces, as indicated.)

through attenuation. Hence the slope of the decay should yield $\alpha_0+\alpha_l$ at that frequency [see Eqs. (1)–(3)], and the value so obtained is marked in the figure.

There are two interesting features in Fig. 9 displayed most clearly by the distribution curves at 0.1 and 0.25 μsec following the termination of the current pulse. Initially the low-frequency flux keeps growing even though the high-frequency flux is being attenuated. This is not really surprising since the flux at the higher pump frequencies is still large initially, and as it is being attenuated a fraction is down converted to feed the much less attenuated lower-frequency flux. Another feature is the slight lag of the low-frequency domain behind the high-frequency one. This lag is seen more clearly in the oscillograms of Fig. 10, where the output of the photomultiplier at the two scattering angles corresponding to 2.5 and 0.28 GHz is displayed as a function of time. The peak on the left records the transit through the light spot of the leading 2.5-GHz domain, while that on the right registers the 0.28-GHz domain. The spatial displacement of about 0.2 mm between the two domains cannot be an experimental artifact since the pair of frequencies chosen corresponds to the same incident angle of the laser beam (and different scattering angles). Thus, an identical volume of the samples is involved in the Brillouin scattering at the two frequencies. At present we have no explanation of this phenomenon but undoubtedly it should play a key role in the understanding of down-conversion processes.

"After-current" measurements similar to those of Fig. 9 were carried out at other low frequencies.

Figure 11 is a semilog plot of the time decay of the peak intensity in the propagating domain at the various frequencies indicated. The current pulse used to generate the low-frequency flux was the same for all frequencies. Here again the decay is exponential over an appreciable range, permitting a fairly accurate determination of the small-signal values of $\alpha_0+\alpha_l$ (marked near each curve). Shortly after the termination of the pulse, however, the decay is faster than exponential for some of the higher frequencies and slower for the lower frequencies. This behavior reflects a rather complex superposition of down- and up-conversion processes.

At higher frequencies ($\gtrsim 0.8$ GHz) the measurements become increasingly more inaccurate be-

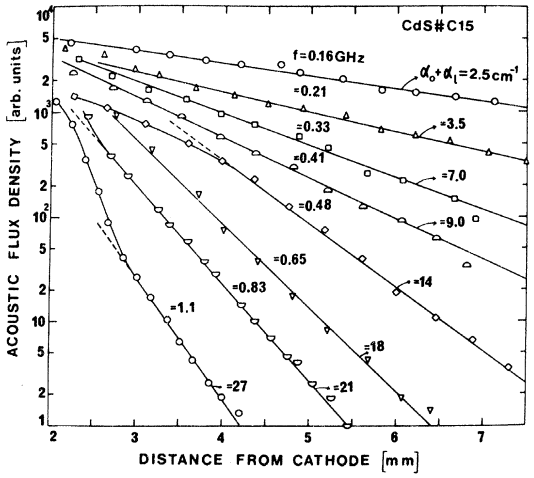


FIG. 11. Time decay of peak flux intensity in propagating domain after termination of short large-amplitude pulse, plotted for different frequencies.

cause of the rapid attenuation. Nevertheless there is a clear indication that the values of $\alpha_0+\alpha_l$ derived from the decay slopes are lower than those indicated by the data of Figs. 7 and 8, in which low-frequency flux is almost entirely absent. In contradistinction, here the flux at low frequencies ($\lesssim 0.6$ GHz) is 1–2 orders of magnitude more intense than that at the medium frequency range. Very likely, then, up conversion is responsible for the slower-than-expected decay of the medium-frequency flux. At the same time, the decay rate of the low-frequency flux is hardly affected by such up conversion because of its much higher intensity.

The after-current measurements described above yield only the sum $\alpha_0(f)+\alpha_l(f)$. In order to determine $\alpha_0(f)$ and $\alpha_l(f)$ separately, low-frequency flux was first generated by a short pulse as before. Some time later, when most of the high-frequency flux had been attenuated, a second pulse was applied. The ratio $\phi_2/\phi_1$ of the peak flux intensity at two positions (separation $\Delta x$) of the propagating domain was then measured as a function of $\gamma$ of the second pulse. In Fig. 12, $\phi_2/\phi_1$ (normalized to $\Delta x = 1$ cm) is plotted against $\gamma$ on a semilog scale for three frequencies. The exponential character of the curves indicates that the propagation takes place under small-signal conditions. One then has $\phi_2/\phi_1 = e^{\alpha_0(\gamma-\gamma_l)}$. Thus the slope of each experimental line yields $\alpha_0$ while its intercept with the horizontal line $\phi_2/\phi_1 = 1$ gives $\gamma_l (\equiv \alpha_l/\alpha_0)$. It should be noted that the thermal flux ($\phi_0$) does not play a direct role in the measurements because $\phi_1$, $\phi_2 \gg \phi_0$. Also, throughout the measurement range, $\gamma$ is below the threshold for net gain. Although for better accuracy in determining $\alpha_l$ it would have been desirable to increase $\gamma$ above threshold ($\phi_2/\phi_1 > 1$), such a procedure results in departures from the small-signal regime. Under the present conditions, the accuracy in $\alpha_l$ is considerably lower than that attained at the high-frequency range (Figs. 7 and 8).

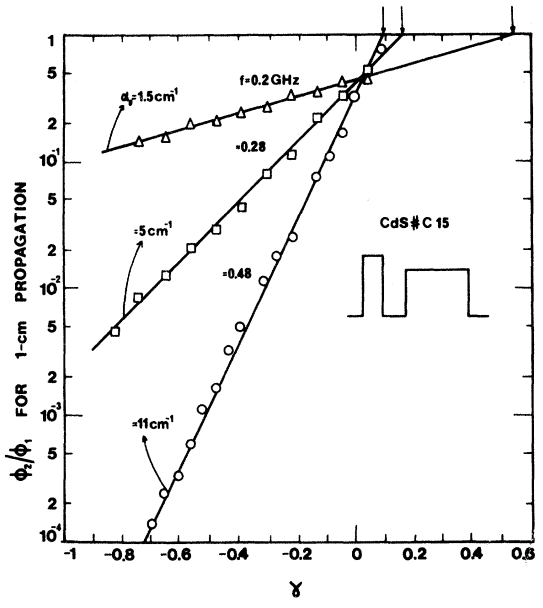


FIG. 12. Ratio $\phi_2/\phi_1$ of peak flux intensities measured at two different positions of propagating domain as function of $\gamma$ of second pulse. Results (normalized to 1-cm propagation) are plotted for three frequencies. Intercepts of straight lines with $\phi_2/\phi_1 = 1$ line (marked by arrows) yield $\gamma_l (\equiv \alpha_0/\alpha_l)$ values. Pulse configuration used is shown by diagram.

Figure 13 summarized our data on the frequency dependence of the field-free amplification factor $\alpha_0$. The circles represent results obtained by amplification of thermal flux around the frequency of maximum net gain (Figs. 7 and 8). The triangles at the low- and medium-frequency ranges were derived from $\gamma$-dependence measurements involving down-converted flux (Fig. 12). The square symbols were obtained from after-current data (Figs. 9 and 11) by subtracting from $\alpha_0+\alpha_l$ the corresponding values of $\alpha_l$ as determined by the $\gamma$-dependence measurements of Fig. 12. Actually in the range 0.2–0.6 GHz, $\alpha_l \approx 1$ cm$^{-1}$ (see Fig. 14 below) and all $\alpha_0+\alpha_l$ values were simply reduced by 1 cm$^{-1}$. In most of this range the inaccuracy in $\alpha_l$ does not introduce a significant error in $\alpha_0$. At the medium-frequency range $\alpha_l \ll \alpha_0$ and no correction is necessary.

The solid curve in Fig. 13 is theoretical, as calculated from Eq. (3) on the basis of the independently measured room-temperature values of the electron concentration and mobility of the CdS sample studied. The only other parameter entering Eq. (3) is the electromechanical coupling constant $K^2$ which has been accurately determined for CdS by measurements of the elastic, piezoelectric, and dielectric tensors.[35] It is seen that the agreement between theory and experiment is good over more than a decade of frequency range. Particularly to be noted is the excellent agreement at the more interesting high-frequency range. In this range small-signal conditions could be strictly maintained throughout. Not so in the intermediate-frequency range (0.8–1.5 GHz) where, as has been explained in connection with Fig. 11, the measurements are hampered by up conversion from the intense low-frequency flux. At the low-frequency range, on the other hand, small-signal conditions can once again be maintained to a good approximation and the small scatter in the points is largely due to experimental errors.

Figure 14 is a log-log plot of the frequency dependence of the lattice attenuation $\alpha_l$. The circles and triangles refer to measurements on two different samples. The upper frequency range of the

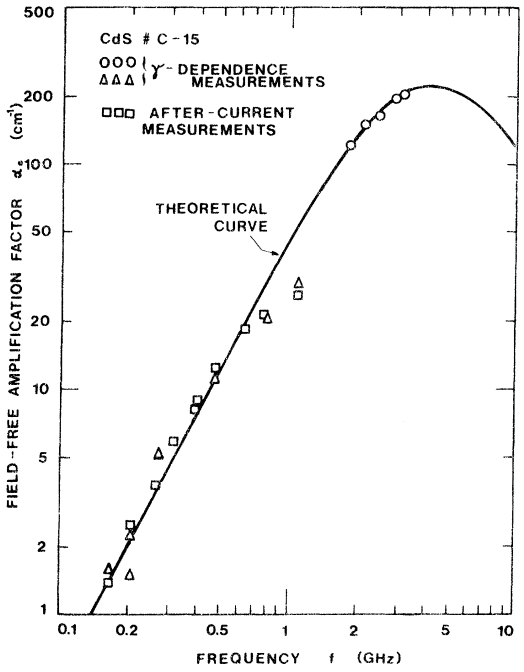


FIG. 13. Frequency dependence of field-free amplification factor $\alpha_0$. Theoretical curve calculated from Eq. (3) for electron concentration ($3.3\times10^{15}$ cm$^{-3}$) and mobility (280 cm$^2$/V sec) of CdS sample studied.

spectrum has been obtained from data of the type shown in Figs. 7 and 8, and the lower range from the measurements of Fig. 12. No values are available for $\alpha_l$ at intermediate frequencies where, as has been pointed out above, small-signal conditions could not very well be attained. The solid line passing through the experimental points has a slope of two in the high-frequency range, typical of Akhiezer attenuation[18] (see below). At low frequencies, on the other hand, $\alpha_l$ varies much more slowly. The errors involved in this range are rather large and better data (in the range 0.1–0.5 GHz) have been obtained by Bateman and McFee[15] from transducer measurements. Actually, the quantity measured in this experiment was $\alpha_0(f) + \alpha_l(f)$, but $\alpha_0(f)$ was unjustifiably neglected. Accordingly, we estimated $\alpha_0(f)$ on the basis of the quoted resistivity of the sample (1 Ωcm) and assuming the mobility to be 300 cm$^2$/V sec, and subtracted this function from Bateman and McFee's data. The curve so obtained is shown in Fig. 14 (dash-dot line). Our results are compatible—within the margin of error—with this curve.

Also included in Fig. 14 are the results obtained by Zucker *et al.*[20] and by Ishida and Inuishi[23] using Brillouin-scattering measurements on semiconducting CdS. Both groups employed a dual-pulse scheme wherein a flux domain is generated by the first pulse and its attenuation studied during the second pulse. In contrast to our measurements, however, no time was allowed to elapse between the two pulses. This procedure has serious drawbacks in that both high and low frequencies, at appreciable flux densities, are simultaneously present in the domain throughout its attenuation. As a consequence up- and down-conversion processes most probably play an important role, so that the measured attenuation of each frequency component may very well not represent the small-signal value. In support of this supposition, we have calculated from the data of Zucker *et al.*[20] and of Ishida and Inuishi[23] the frequency dependence of $\alpha_0$. The results deviate badly from the theoretical curve, at some frequencies by as much as a factor of 5. Finally, we have included in Fig. 14 the results of Siebert *et al.*[11] obtained for *inactive* shear waves in CdS, in which both the polarization and direction of propagation are normal to the *c* axis. The $\alpha_l(f)$ curve shows an $f^{1.5}$ dependence in contrast to our $f^2$ dependence. However, there is not much point in comparing the two sets of data since the attenuation is expected to be different for the two polarization modes, as has indeed been observed for example in germanium.[16,36]

Once the frequency dependence of the lattice attenuation $\alpha_l$ has been determined, one can compare the measured spectrum of the amplified flux with the spectrum predicted by the small-signal theory. Such comparison is shown in Fig. 15 for two different values of $\alpha_n(f_N)v_s t$. The experimental points correspond to the plateau of the spatial distribution ($x > v_s t$) and were obtained by the dou-

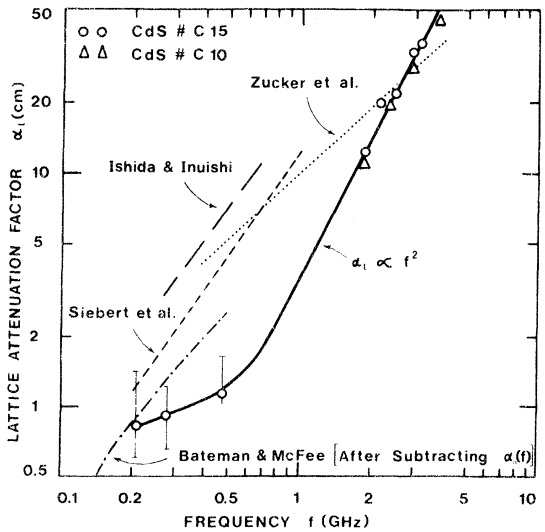


FIG. 14. Frequency dependence of lattice attenuation $\alpha_l$. Circles and triangles refer to two different CdS samples. Solid curve passing through experimental points has slope of two ($f^2$ dependence) at high-frequency range. Also included are data obtained by other works (see text).

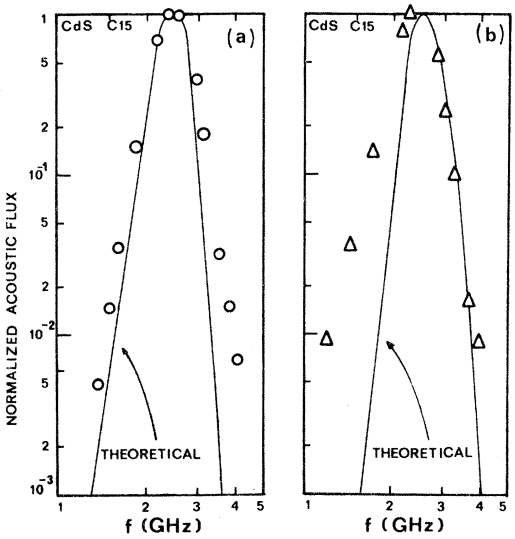


FIG. 15. Frequency spectrum of amplified flux in plateau region ($x > v_s t$). (a) Weak flux conditions, $\alpha_n(fN)v_s t = 12$. (b) Higher flux level, $\alpha_n(f_N)v_s t = 16$. Theoretical curve calculated from Eqs. (3) and (4b) on basis of sample's parameters ($n$, $\mu$) and experimentally determined $\alpha_l(f)$ function (Fig. 14). Experimental values and theoretical curves normalized to unity at maximum intensity. Spectral resolution better than 40 MHz.

ble-pulse technique. The theoretical curve was calculated from Eqs. (3) and (4b) on the basis of the sample's parameters ($n$, $\mu$) and the experimentally determined $\alpha_l(f)$ function. A Debye $f^2$ dependence has been assumed for the thermal flux density $\phi_0$ but this plays an insignificant role in the shape of the theoretical curve. In particular, the frequency of maximum *intensity* is hardly distinguishable from the frequency of maximum *net gain*. Both the experimental and theoretical values have been normalized to unity at maximum flux density. For the spectrum of Fig. 15(a), which corresponds to weak-flux conditions, the agreement between theory and experiment is quite good. It should be stressed that no adjustable parameters were used in this fit. The fact that the observed frequency of maximum intensity (2.5 GHz) coincides with the calculated value of the frequency of maximum net gain $f_N$ is further indication for the $f^2$ dependence of $\alpha_l$ used in the calculation.

The spectrum in Fig. 15(b) has been obtained under higher flux densities (by about one order of magnitude). Departures from the theoretical curve are now apparent, with down conversion to lower frequencies beginning to take place. Such down conversion is, however, considerably less pronounced than within a domain of comparable flux density. As we pointed out elsewhere,[13] it is believed that this difference in behavior is due to the fact that in the latter case shock-excited low-frequency flux acts as the stimulating signal for the down conversion of the pump frequencies (around $f_N$), whereas in the former case ($x > v_s t$) the signal consists of the much weaker thermal flux. This and other aspects of nonlinear interactions are now under investigation.

## CONCLUSION

In this work the small-signal theory of acoustoelectric amplification in CdS has been quantitatively verified for the first time in the GHz range. Good agreement, but not as detailed, between theory and experiment has already been demonstrated at low frequencies (50–500 MHz) by transducer measurements on photoconducting CdS.[14] It appears then that, as expected, the basic assumption underlying the theory, namely, that the electron momentum relaxation time is energy independent, is a good one in the regime $ql \ll 1$. The only other high-frequency data amenable to quantitative comparison with the small-signal theory were those obtained by Palik and Bray[8] for $n$-GaAs in the regime $ql \approx 1$. The experimental values of $\alpha_0(f)$ were found to lie about 20% below the theoretical curve. Whether this discrepancy is due to the effect of the energy dependence of the relaxation time, which may be appreciable[37] for $ql \approx 1$, or to uncertainty in the values of the sample's parameters and/or homogeneity could not be determined by these authors.

Most of the previous measurements[9,20,23,24] on CdS involved domains where strict small-signal conditions are very difficult to maintain. We believe that the results reported[20,23] for $\alpha_l(f)$ reflect to a greater or lesser extent effects associated with nonlinear processes. Our results, especially in the high-frequency range (around $f_N$), are free of this limitation. In this range $\alpha_l$ is found to follow an $f^2$ Akhiezer law expected to hold when the relaxation time $\tau_{th}$ of the thermal phonons with which the acoustic flux interacts is small compared to $1/2\pi f$.[16–19] Unfortunately, however, there is no direct way of determining $\tau_{th}$ and through it the range of validity of the $f^2$ law. Instead, $\tau_{th}$ is commonly estimated from the thermal conductivity even though it is doubtful whether the same phonons are involved in both the thermal conductivity and the acoustic attenuation. For CdS, two estimates are available (at room temperature) for $\tau_{th}$, $7\times10^{-12}$ sec[38] and $3\times10^{-11}$ sec,[39] for both of which $2\pi f\tau_{th} < 1$ in our frequency range. Although an $f^2$ dependence has been observed in several materials, deviations from this law are more commonly encountered.[8] The proportionality factor between $\alpha_l$ and $f^2$ depends on complicated averages[38,40] of the Grüneisen constant $\gamma_G$. Experimentally we find that $\alpha_l/f^2 = 3.6$ cm$^{-1}$ GHz$^{-2}$. This result com-

bined with heat-conductivity data[41] leads[19] to a value of 0.35 for $\gamma_G$.

At low frequencies ($\lesssim 0.5$ GHz) our results, as well as those obtained by transducer measurement,[15] show a weaker dependence of $\alpha_l$ on $f$. The attenuation at these frequencies is very low (around 1 $cm^{-1}$) and $\alpha_l$ may well be governed by structure sensitive factors of unknown frequency dependence. It would be highly desirable to carry out measurements on samples of higher perfection to check whether the $f^2$ dependence of the *intrinsic* lattice attenuation in CdS extends, as it should, to lower frequencies.


## ACKNOWLEDGMENTS

The authors wish to thank D. Freyhan for constructing the electronic apparatus and the members of the Fine Mechanics Workshop under the direction of A. Shirizly for building the mechanical parts.



[1]A. R. Hutson and D. L. White, J. Appl. Phys. 33, 40 (1962).

[2]J. H. McFee, in *Physical Acoustics IV*, edited by W. P. Mason (Academic, New York, 1966), Part A, p. 1.

[3]A. Many and I. Balberg, in *Electronic Structure in Solids*, edited by E. D. Haidemanakis (Plenum, New York, 1969), p. 385.

[4]For a review and other references pertaining to Brillouin-scattering measurements, see N. I. Meyer and M. H. Jørgensen, in *Advances in Solid State Physics* (Pergamon, Vieweg, 1970), p. 21.

[5]J. Zucker and S. Zemon, Appl. Phys. Letters 9, 398 (1966).

[6]W. Wettling, Phys. Letters 25A, 193 (1967).

[7]D. L. Spears, Phys. Rev. B 2, 1931 (1970).

[8]E. D. Palik and R. Bray, Phys. Rev. B 3, 3302 (1971).

[9]J. Zucker and S. Zemon, J. Phys. Chem. Solids 31, 1673 (1970).

[10]J. Zucker and S. Zemon, J. Acoust. Soc. Am. 49, 1037 (1971).

[11]F. Siebert, O. Keller, and W. Wettling, Phys. Status Solidi 4, 67 (1971).

[12]H. Kusmany and W. Liederen, in *Light Scattering in Solids*, edited by M. Balkanski (Flammarion, Paris, 1971), p. 473.

[13]A. Many and U. Gelbart, Appl. Phys. Letters 19, 192 (1971).

[14]D. L. White, E. T. Handelman, and J. T. Hanlon, Proc. IEEE 53, 2157 (1965).

[15]T. B. Bateman and J. H. McFee, J. Appl. Phys. 39, 4471 (1968).

[16]M. Pomerantz, Proc. IEEE 53, 1438 (1965).

[17]M. G. Holland, IEEE Trans. Sonics Ultrasonics SU-15, 18 (1968).

[18]A. Akhiezer, J. Phys. (USSR) 1, 277 (1939).

[19]T. O. Woodruff and H. Ehrenreich, Phys. Rev. 123, 1553 (1961).

[20]J. Zucker, S. A. Zemon, and J. H. Wasko, in *Proceedings of the Ninth International Conference on the Physics of Semiconductors*, Moscow, 1968 (Nauka, Leningrad, 1968), Vol. 2, p. 904.

[21]H. N. Spector, Phys. Rev. 165, 562 (1968).

[22]J. Yamashita and K. Nakamura, in *Proceedings of the Tenth International Conference on the Physics of Semiconductors*, Cambridge, Mass., 1970, edited by S. P. Keller, J. C. Hensel, and F. Stern (U.S. AEC, Division of Technical Information Extention, Oak Ridge, Tennessee, 1970), p. 694.

[23]A. Ishida and Y. Inuishi, J. Phys. Soc. Japan 27, 911 (1969).

[24]G. I. Robertson and M. B. N. Butler, Electronics Letters 5, 529 (1969).

[25]G. D. Benedek and K. Fritsch, Phys. Rev. 149, 647 (1966).

[26]R. W. Dixon, IEEE J. Quantum Electronics QE-3, 85 (1967).

[27]L. L. Hope, Phys. Rev. 166, 883 (1968).

[28]E. J. Jacobsen, J. Acoust. Soc. Am. 32, 949 (1960).

[29]R. O. Sliva and R. Bray, Phys. Rev. Letters 14, 372 (1965).

[30]R. Bray, IBM J. Res. Develop. 13, 487 (1969).

[31]B. Fisher, B. Pratt, J. Gorelick, I. Feingold, and A. Many, J. Appl. Phys. 43, 3607 (1972).

[32]It should be pointed out that in GaAs, and more so in InSb, the values of $\alpha_0$ are much smaller. As a result the $\gamma$ values used are correpondingly larger so that the gain is much less sensitive to the sample's inhomogeneity.

[33]A. Many and I. Balberg, Phys. Letters 24A, 705 (1967); I. Balberg and A. Many, Phys. Letters 24A, 707 (1967).

[34]R. W. Smith, J. Acoust. Soc. Am. 49, 1033 (1971).

[35]D. Berlincourt, H. Jaffe, and L. R. Shiozawa, Phys. Rev. 129, 1009 (1963).

[36]M. Pomerantz, IEEE Trans. Sonics Ultrasonics SU-11, 68 (1964).

[37]C. Jacoboni and E. H. Prohofsky, Phys. Rev. B 1, 697 (1970).

[38]M. F. Lewis, J. Acoust. Soc. Am. 43, 852 (1968).

[39]A. S. Pine, Phys. Rev. B 5, 2997 (1972).

[40]W. P. Mason and T. B. Bateman, J. Acoust. Soc. Am. 36, 644 (1964).

[41]M. G. Holland, Phys. Rev. 134, A471 (1964).